Journal of Materials Chemistry C

# Highly stable and efficient deep-red phosphorescent organic light-emitting devices using phenanthroline derivative as n-type exciplex host partner

SCHOLARONE™
Manuscripts

**Highly stable and efficient deep-red phosphorescent organic light-emitting devices using phenanthroline derivative as n-type exciplex host partner**

*By Hisaki Tsuneyama, Hisahiro Sasabe*, Yu Saito, Taito Noda, Daiki Saito, Junji Kido**

[*] Prof. H. Sasabe, Prof. J. Kido
Research Center for Organic Electronics (ROEL), Yamagata University, 4-3-16 Jonan, Yonezawa, Yamagata 992-8510, Japan; Frontier Center for Organic Materials (FROM), Yamagata University, 4-3-16 Jonan, Yonezawa, Yamagata 992-8510, Japan
E-mail: (h-sasabe@yz.yamagata-u.ac.jp, kid@yz.yamagata-u.ac.jp)

Prof. H. Sasabe, Prof. J. Kido, H. Tsuneyama, Y. Saito, T. Noda, D. Saito
Department of Organic Materials Science, Graduate School of Organic Materials Science, Yamagata University, 4-3-16 Jonan, Yonezawa, Yamagata 992-8510, Japan

**Abstract**

Although deep-red illumination light sources with an emission peak wavelength over 660 nm are optimal for plant growing and health monitoring systems, the stability and efficiency of organic light-emitting diodes (OLEDs) is insufficient for practical applications. In this study, we developed a novel exciplex host system to realize highly stable and efficient deep-red OLEDs by utilizing **nBPhen**, a phenanthroline derivative, as the n-type exciplex host partner and combined **(DPQ)$_2$Ir(dpm)**, a deep-red iridium complex, and **α-NPD**, a conventional triarylamine derivative, as the p-type exciplex host partner. The proposed optimized device exhibits a lifetime that is 6.6 times longer when compared with the state-of-the-art deep-red OLEDs and maintains a high maximum external quantum efficiency of approximately 17% at a low operating voltage of 2.37 V; such performance is considered among the best in the scientific literatures.

## 1. Introduction

Organic light-emitting diodes (OLEDs) are considered as promising devices for next generation illumination light sources due to unique features that include low power consumption, thin paper-like thickness and flexibility, and area light sources.[1] Among visible light regions, deep-red OLEDs with an emission peak wavelength of over 660 nm are in high demand, especially for horticulture and health monitoring systems; however the stability and efficiency of these devices is insufficient for practical applications.[2]

To demonstrate recent and relevant examples, in 2020, Chi and co-workers developed a series of square-planar Pt (II) complexes showcasing deep-red/near infrared (NIR) emissions with a peak wavelength of around 660–680 nm.[3] These complexes formed oligomer with ease and exhibited strong aggregation-induced emission upon realizing a maximum external quantum efficiency (EQE) of ~30%. However, the stability of these devices has not been reported. In the same year of 2020, Wong and co-workers reported a series of deep-red to NIR emitting iridium complexes.[4] These emitters exhibited moderate photoluminescence quantum yields (PLQY) of ca. 45% with a PL emission peak of around 700 nm in **CBP**, a carbazole-based host matrix. The corresponding OLED exhibited a maximum EQE of 10.6%, and a lifetime of 17 hours at 50% initial luminance ($LT_{50}$) at the initial luminance of 114 cd m$^{-2}$. In 2018, Yasuda and co-workers reported a series of highly efficient red thermally activated delayed fluorescence (TADF) emitters.[5] Among these emitters, **Da-CNBPz** exhibited an EQE of 15% at an EL peak wavelength of 670 nm using **CBP** as a host material, along with $LT_{50}$ of 106 hours at the initial luminance of 100 cd m$^{-2}$. As demonstrated above, although a few deep-red OLEDs exhibited extremely high EQE, their lifetime is limited and insufficient for the practical applications.

To resolve this shortcoming, Sasabe and Kido focused on the host material since **CBP**, a wide energy-gap host material, is not utilized in OLEDs with longer lifetimes, but frequently utilized in deep-red OLEDs.[6] They proposed to employ the narrow gap exciplex system based on a triarylamine-based p-type host and a triphenyltriazine-based (**DBT-TRZ**) n-type host partner.

2

By employing bis(2,3-diphenylquinoxaline)iridium(dipivaloylmethane) [(**DPQ)₂Ir(dpm)**], a deep-red iridium complex in the exciplex host system, the optimized device exhibited an EL peak wavelength of 670 nm and EQE of 12% along with a longer lifetime at 80% initial luminance ($LT_{80}$) of approximately 1500 hours at an initial luminance of approximately 300 cd m$^{-2}$ (current density: 25 mA cm$^{-2}$).[6c] However, the n-type host material **DBT-TRZ** exhibited a shallow electron affinity ($E_a$) of −2.8 eV that is 1.0 eV shallower than that of the emitter ($E_a$ = −3.8 eV), thereby causing the loss of carrier balance and the high-operating voltages. In addition, the potential electromer formation of the triphenyltriazine derivative may limit the operational lifetime.[7] Therefore, a thermally and electrically stable n-type host material based on a non-triphenyltriazine derivative with deeper $E_a$ is considered to be a more suitable alternative.

In this study, we developed a novel exciplex host system for realizing highly stable and efficient deep-red OLEDs using **nBPhen,** a phenanthroline derivative, as the n-type exciplex host partner with a deep-red phosphorescent emitter, **(DPQ)₂Ir(dpm)**. For the the p-type exciplex host partner, we used a conventional triarylamine derivative, **α-NPD**. The optimized device exhibited a 6.6 times longer lifetime compared to the state-of-the-art deep-red OLEDs, while maintaining a maximum EQE of approximately 17%. These performances are among the best in the current scientific literatures.

## 2. Result and Discussion

### 2.1. Selection of the n-type host partners and DFT calculations

As mentioned in the introduction, the typical triphenyltriazine-based n-type host material has shallow $E_a$ compared with that of the deep-red emitter **(DPQ)₂Ir(dpm)** ($E_a$ = −3.8 eV), resulting in the loss of carrier balance and high-operating voltages. Moreover, the potential electromer formation of the triphenyltriazine derivative may limit the operational lifetime. Therefore, a non-triphenyltriazine based n-type host material with deeper $E_a$ can be a more suitable

alternative. To meet these prerequisites, we selected three types of phenanthroline derivatives, **nBPhen**, **DPB**[8], and **pDPB**. These materials are frequently utilized as an electron-transporter in long lifetime OLEDs.[9] It should be noted that only a limited number of researchers have used 1,10-phenanthroline derivatives such as **BPhen** and **β-BNPhen** as the n-type exciplex partner to prolong the stability of yellow-to-orange phosphorescent OLEDs.[10]

 First, we conducted density functional theory (DFT) calculations to predict the frontier molecular orbital (FMO) levels such as the highest occupied molecular orbital (HOMO) level, the lowest unoccupied molecular orbital (LUMO) level, and the excited triplet level ($E_T$) using the computational chemistry software package Gaussian 09.[11] **Figure 1** displays the calculation results. The electron clouds of FMOs were distributed on the phenanthroline skeletons expecting the superior molecular packing to lead to favorable charge mobility. All the phenanthroline derivatives exhibited a sufficiently high $E_T$ of over 2.3 eV compared to the deep-red emitter ($E_T$ = 1.95 eV).


## 2.2. Thermal and photophysical properties

   The thermal stability of the emitters was investigated using thermal gravimetric analysis (TGA) and differential scanning calorimetry (DSC) (**Figures S1-S6**, Supporting Information). These emitters exhibited high thermal stability with a weight of loss 5% ($T_{d5}$) at temperatures of over 475 °C. **nBPhen** exhibited a high glass transition temperature ($T_g$) of 149 °C. However, $T_g$ was not observed in **DPB** and **pDPB**, indicating that these compounds have high crystallinity. To further evaluate the thermal stability in the vacuum deposited thin films, we investigated the atomic force microscope (AFM) images that were obtained immediately after deposition and after exposure to the ambient atmosphere for 24 hours (**Figure S7**). After deposition, **nBPhen** and **pDPB** displayed smooth surfaces with root-mean-square roughness ($R_{rms}$) within 1.6 nm, whereas **DPB** exhibited a rough surface with $R_{rms}$ of over 8.0 nm, thereby indicating high crystallinity. After exposure to the ambient atmosphere for 24 hours, **nBPhen** continued to

exhibit a smooth surface, whereas **pDPB** displayed a rough surface with some needle-like microcrystal growth and an $R_{rms}$ of over 3.0 nm. These AFM observations indicated that the order of the crystallinity was **nBPhen** < **pDPB** < **DPB**. To investigate the photophysical properties, the ionization potentials ($I_p$) were measured using the photoelectron yield spectroscopy (PYS). The $I_p$ values were respectively obtained as –6.3 eV and –6.2 eV for **nBPhen** and **pDPB**. The energy gap ($E_g$) estimated from the UV absorbance edge are displayed in **Figure 2** and **Figure S3-S4**. The $E_a$ value was calculated as –3.3 eV for **nBPhen** and –3.1 eV for **pDPB** by subtracting the optical $E_g$ from the $I_p$ levels. It should be noted that we used the photophysical properties of **DPB** reported in the reference.[8] These phenanthroline derivatives exhibited deep $E_a$ values that was 0.2–0.3 eV deeper than triphenyltriazine-based n-type host partner, **DBT-TRZ** ($E_a$ = –2.8 eV). The $E_T$ values were estimated to be 2.37 eV for **nBPhen**, 2.47 eV for **DPB**, 2.92 eV for **pDPB** from the onset of phosphorescence spectra in dilute 2-methyltetrahydrofuran (2-MeTHF) or dilute toluene solutions (**Figure S8-S10)**. As predicted by the DFT calculations, these phenanthroline derivatives exhibited sufficiently high $E_T$ levels when compared with the deep-red emitter **(DPQ)₂Ir(dpm)** ($E_T$ = 1.95 eV). All the thermal and photophysical properties are summarized in **Table 1**.

### 2.3. Photophysical properties of the co-deposited film

To validate the formation of exciplex between **α-NPD** and these phenanthroline derivatives, we measured the UV-Vis absorption spectra and the PL spectra for the co-deposited film of **α-NPD**: phenanthroline derivatives (1:1 molar ratio) as displayed in **Figure 2**. The UV-Vis absorption of the **α-NPD/nBPhen** co-deposited film demonstrated a spectrum that was similar to the sum of each single film with no derivable absorption peak from the CT complex that could be observed in the long wavelength region. In contrast, for the PL spectrum, a new emission peak appeared at 492 nm on the longer wavelength side of each single film. Similar results were obtained from the UV-Vis absorption and PL spectra of the co-deposited films of

**α-NPD/DPB** and **α-NPD/pDPB** (**Figures S11** and **S12**), thereby confirming that these phenanthroline derivatives could form an exciplex with **α-NPD** and act as the n-type host partner. Thereafter, we evaluated these exciplexes as hosts for the deep-red phosphorescent emitter **(DPQ)₂Ir(dpm)**. We fabricated the vacuum deposition films of these exciplex hosts doped with 1 wt.% **(DPQ)₂Ir(dpm)** and measured the photoluminescence quantum yields (PLQY). The PLQY values were measured to be between 45–57%, which is similar to the values obtained in the **α-NPD/DBT-TRZ** exciplex host (PLQY = 54%).[6a]

### 2.4. OLED performance (I)

To evaluate the performance of these phenanthroline derivatives as n-type host materials, three types of OLED devices were fabricated using **(DPQ)₂Ir(dpm)** as an emitter wherein 8-quinolinolato lithium (Liq) was employed as the electron injection layer. The device structure was a simple structure with few interfaces as follows: ITO (130 nm)/polymer buffer[12] (20 nm)/**NPD** (20 nm)/exciplex host doped with 1 wt.% **(DPQ)₂Ir(dpm)** (40 nm)/phenanthroline derivatives (50 nm)/ 20 wt.% Liq doped phenanthroline derivatives (20 nm)/Liq (1 nm)/Al (80 nm). The energy diagram and chemical structure of materials used in the structure are displayed in **Figure 3**. The OLED performances are summarized in **Figure 4** and **Table 2**. **Figure 4(a)** illustrates the EL spectra at 1 mA. All the devices exhibited an emission peak at around 670 nm, along with a very small emission peak at 500–550 nm that could be attributed to the emission from the exciplex. This was most likely due to the insufficient energy transfer, especially for **nBPhen** from the exciplex host to the emitter. Among these three phenanthroline derivatives, the **nBPhen**-based device provided the lowest turn-on voltage at 1 cd m⁻² ($V_{on}$) of 2.41 V; it was most likely due to the deeper $E_a$ of **nBphen** achieving a superior electron injection from the cathode. All the devices exhibited high maximum EQE of over 14% with a small efficiency roll-off. Thereafter, we measured the operational lifetime of the devices under a constant current density of 25 mA cm⁻². The **nBPhen**-based device exhibited a much longer

lifetime of $LT_{80}$ of 640 hours. These results were attributed to the high thermal stability of the thin film with $T_g$ of approximately 150 °C, and the superior electron transport characteristics of **nBPhen**. To further investigate the elecctron transport characteristics of phenanthroline derivatives, we made electron-only devices w/ and w/o p-type host partner (**Figure S13, 14**). The order of the current densities were same in both systems as **nBPhen** > **DPB** > **pDPB**. These results clearly show the superior electron transport characteristics of **nBPhen** compared with **DPB** and **pDPB**. The **DPB** and **pDPB**-based devices exhibited shorter operational lifetimes of 34.3, and 0.30 hours, respectively. A possible reason for the low device stability could be attributed to the highly crystalline nature of the individual films and inferior electron transport characteristics.

## 2.5. OLED performance (II)

As mentioned above, the **nBPhen**-based device achieved a high EQE of approximately 17% and a long operational lifetime of $LT_{80}$ of 640 hours under a constant current density of 25 mA cm$^{-2}$. However, a weak emission peak from the exciplex suggested an inefficient energy transfer between the exciplex host and the guest emitter. Therefore, the efficiency and lifetime of the device could be improved further. As a result, we investigated the effect of doping concentration on the OLED performance by changing the concentration from a range of 1 to 10 wt.%. **Figure 5** displays the device characteristics, and **Table 3** summarized all the performances. **Figure 5(a)** demonstrates the EL spectra results at 1 mA. The emission from the exciplex host decreased when the doping concentration increased from 1 to 3 wt.% suggesting the efficient energy transfer from the exciplex host to the emitter, which significantly contributes to improve the device lifetime (**Figure 5(d)**)[6]. Further increase of the doping concentration induced a slight redshift in the emission peak of **(DPQ)₂Ir(dpm)**. The maximum EQE of 16.7% was recorded in the device at the doping concentration of 3 wt.%. However, EQE decreased as the doping concentration increased further, primarily due to concentration quenching. In addition,

PLQY of the co-deposited films gradually decreased with the increase in the doping concentration (PLQY = 56% for 3 wt.%, and 45% for 10 wt.%). Furthermore, measuring the operational lifetime of the device under a constant current density of 25 mA cm$^{-2}$ revealed that $LT_{80}$ extended substantially with the increase in doping concentration from 3800 hours for 3 wt.% to 9840 hours for 10 wt.%. These obtained values of operational lifetime of the device was approximately 6.6 times longer than that of the previous state-of-the-art devices.[6c]

Further, we investigated the effect of p:n ratio of the exciplex host system on the device performance. Herein, the doping concentration of the emitter was fixed at 3 wt.% since it exhibited high efficiency and a longer lifetime simultaneously. We changed the ratio of p/n hosts to 67:33, 40:60, and 30:70. The results of these ratio changes on the device characteristics are presented in **Figure S15** and **Table S1**. As the proportion of n-type host increased, the current density and the efficiency decreased gradually because the reduced p-type host proportion could cause the reduced hole carrier density causing the carrier imbalance. The operational lifetime increased further as the proportion of n-type host increased. This can be considered that the increased n-type host partner induced an increase in the electron density, thereby preventing chemical degradation of the p-type host partner. In addition, the broadening of the exciton recombination zone could also contribute to the improvement of the device stability.[7] These results strongly suggest that one of the bottlenecks of operational lifetime is the electrochemical instability of the p-type exciplex host partner toward anion state.

## 3. Conclusions

In conclusion, we proposed phenanthroline derivatives as a novel n-type exciplex host partner with deep $E_a$ level of approximately −3.3 eV that is much deeper than the conventional triphenyltriazine-based n-type host for deep-red OLEDs to realize high-efficiency and longer lifetime. Among three phenanthroline derivatives, **nBPhen** with a high thermal stability in the form of a thin film exhibited superior device performances when combined with **α-NPD** as a

p-type host partner. A deep-red OLED based on **(DPQ)₂Ir(dpm)** using α-**NPD/nBPhen** as the exciplex host system exhibited a high EQE of approximately 17% and low $V_{on}$ of 2.37 V along with a long lifetime of $LT_{80}$ of 9840 hours under a high constant current density of 25 mA cm$^{-2}$. This lifetime is 6.6 times longer than the state-of-the-art deep-red OLEDs while maintaining the high EQE and low operating voltages. Investigating the effect of the p:n ratio of the exciplex host system revealed that the increasing the n-type host partner induced an increase of electron density that caused chemical degradation of p-type host partner. This strongly suggest that the chemical instability of the p-type exciplex host partner toward anion state is one of the bottlenecks to prolong operational lifetime, thereby indicating further scope of improvement by using a chemically stable p-type host partner. We believe that our findings will contribute the rapid development of deep-red OLEDs for display applications as well as illumination light sources for horticulture and health monitoring systems.

**Supporting Information**

Supporting information is available.

**Acknowledgements:**

**References**

1   (a) J. Kido, M. Kimura, K. Nagai, *Science* **1995**, 267, 1332; (b) Y. Sun, N. C. Giebink, H. Kanno, B. Ma, M. E. Thompson, S. R. Forrest, *Nature* **2006**, 440, 908; (c) B. W. D'Andrate, J. Esler, C. Lin, V. Adamovich, S. Xia, M. S. Weaver, R. Kwong, J. J. Brown, *Proc. SPIE* **2008**, 7051, 70510Q–1; (d) S. Reineke, F. Lindner, G. Schwartz, N. Seidler, K. Walzer, B. Lussem, K. Leo, *Nature* **2009**, 459, 234; (e) K. Walzer, B. Maennig, M. Pfeiffer, K. Leo, *Chem. Rev.* **2007**, 107, 1233; (f) H. Sasabe, J. Kido, *J. Mater. Chem. C* **2013**, 1, 1699; (g) H. Uoyama, K. Goushi, K. Shizu, H. Nomura, C. Adachi, *Nature* **2012**, 492, 234 ; (h) C. Adachi, *Jpn. J. Appl. Phys.* **2014**, 53, 060101; (i) Z. Yang, Z. Mao, Z. Xie, Y. Zhang, S. Liu, J. Zhao, J. Xu, Z. Chi, M. P. Aldred, *Chem. Soc. Rev.* **2017**, 46, 915; (j) Y. Im, M. Kim, Y. J. Cho, J.-A Seo, K. S. Yook, J. Y. Lee, *Chem. Mater.* **2017**, 29, 1946; (k) M. Y. Wong, E. Z.-Colman, *Adv. Mater.* **2017**, 29, 1605444; (k) K.-H. Kim, J.-J. Kim, *Adv. Mater.* **2018**, 30, 1705600.

2   (a) J. H. Jou, C. C. Lin, T. H. Li, C. J. Li, S. H. Peng, F. C. Yang, K. R. J. Thomas, D. Kumar, Y. Chi, B. D. Hsu, *Materials* **2015**, *8*, 5265. (b) T. Yamanaka, H. Nakanotani, S. Hara, T. Hirohata, C. Adachi, *Appl. Phys. Exp.* **2017**, *10*, 074101. (c) Y. Sun, X. Yang, Z. Feng, B. Liu, D. Zhong, J. Zhang, G. Zhou, Z. Wu, *ACS Appl. Mater. Interfaces* **2019**, *11*, 26152. (d) Y.-M. Jing, F.-Z. Wang, Y.-X. Zheng, J.-L. Zuo, *J. Mater. Chem. C*, **2017**, *5*, 3714.

3   (a) W.-C. Chen, C. Sukpattanacharoen, W.-H. Chen, C.-C. Huang, H.-F. Hsu, D. Shen, W.-Y. Hung, N. Kungwan, D. Escudero, C.-S. Lee, and Y. Chi, *Adv. Funct. Mater.* **2020**, 2002494. (b) K. T. Ly, R.-W. Chen-Cheng, H.-W. Lin, Y.-J. Shiau, S.-H. Liu, P.-T. Chou, C.-S. Tsao, Y.-C. Huang, and Y. Chi, *Nature Photon.* **2017**, *11*, 63.

4   Z. Chen, H. Zhang, D. Wen, W. Wu, Q. Zeng, S. Chen, and W.-Y. Wong, *Chem. Sci.* **2020**, *11*, 2342.

5   R. Furue, K. Matsuo, Y. Ashikari, H. Ooka, N. Amanokura, and T. Yasuda, *Adv. Optical*

*Mater*. **2018**, *6*, 1701147.

6    (a) Y. Nagai, H. Sasabe, J. Takashi, N. Onuma, T. Ito, S. Ohisa, and J. Kido, *J. Mater. Chem. C,* **2017**, *5,* 527-530. (b) T. Ito, H. Sasabe, Y. Nagai, Y. Watanabe, N. Onuma, and J. Kido, *Chem. Eur. J*. **2019**, *25*, 7308-7314. (c) D. Saito, H. Sasabe, T. Kikuchi, T. Ito, H. Tsuneyama, and Junji Kido, *J. Mater. Chem. C*, **2021**, *9*, 1215-1220.

7    M. Tanaka, H. Noda, H. Nakanotani, and C. Adachi, *Adv. Electron. Mater*. **2019**, 1800708.

8    Y.-J. Pu, G. Nakata, H. Satoh, H. Sasabe, D. Yokoyama, J. Kido, *Adv. Mater*. **2012**, 24, 1765.

9    Z. Wang, M. Li, L. Gan, X. Cai, B. Li, D. Chen, and S.-J. Su, *Adv. Sci*. **2019**, *6*, 1802246.

10   (a) G. Jin, J.-Z. Liu, J.-H. Zou, X.-L. Huang, M.-J. He, L. Peng, L.-L. Chen, X.-H. Zhu, J. Peng, Y. Cao, Science Bulletin 63 (2018) 446-451. (b) Z. Bin, D. Shi, R. Su, W. Han, D. Zhang, and L. Duan, Science Bulletin 65 (2020) 153-160.

11   *Gaussian 09*, Revision D.01, M. J. Frisch, G. W. Trucks, H. B. Schlegel, G. E. Scuseria, M. A.  Robb, J. R. Cheeseman, G. Scalmani, V. Barone, B. Mennucci, G. A. Petersson, H. Nakatsuji, M. Caricato, X. Li, H. P. Hratchian, A. F. Izmaylov, J. Bloino, G. Zheng, J. L. Sonnenberg, M. Hada, M. Ehara, K. Toyota, R. Fukuda, J. Hasegawa, M. Ishida, T. Nakajima, Y. Honda, O. Kitao, H. Nakai, T. Vreven, J. A. Montgomery, Jr., J. E. Peralta, F. Ogliaro, M. Bearpark, J. J. Heyd, E. Brothers, K. N. Kudin, V. N. Staroverov, R. Kobayashi, J. Normand, K. Raghavachari, A. Rendell, J. C. Burant, S. S. Iyengar, J. Tomasi, M. Cossi, N. Rega, J. M. Millam, M. Klene, J. E. Knox, J. B. Cross, V. Bakken, C. Adamo, J. Jaramillo, R. Gomperts, R. E. Stratmann, O. Yazyev, A. J. Austin, R. Cammi, C. Pomelli, J. W. Ochterski, R. L. Martin, K. Morokuma, V. G. Zakrzewski, G. A. Voth, P. Salvador, J. J. Dannenberg, S. Dapprich, A. D. Daniels, Ö. Farkas, J. B. Foresman, J. V. Ortiz, J. Cioslowski, and D. J. Fox, Gaussian, Inc., Wallingford CT, 2013.

12   J. Kido, G. Harada, M. Komada, H. Shionoya, K. Nagai, *ACS. Synp. Ser*. **1997**, *672*, 381.
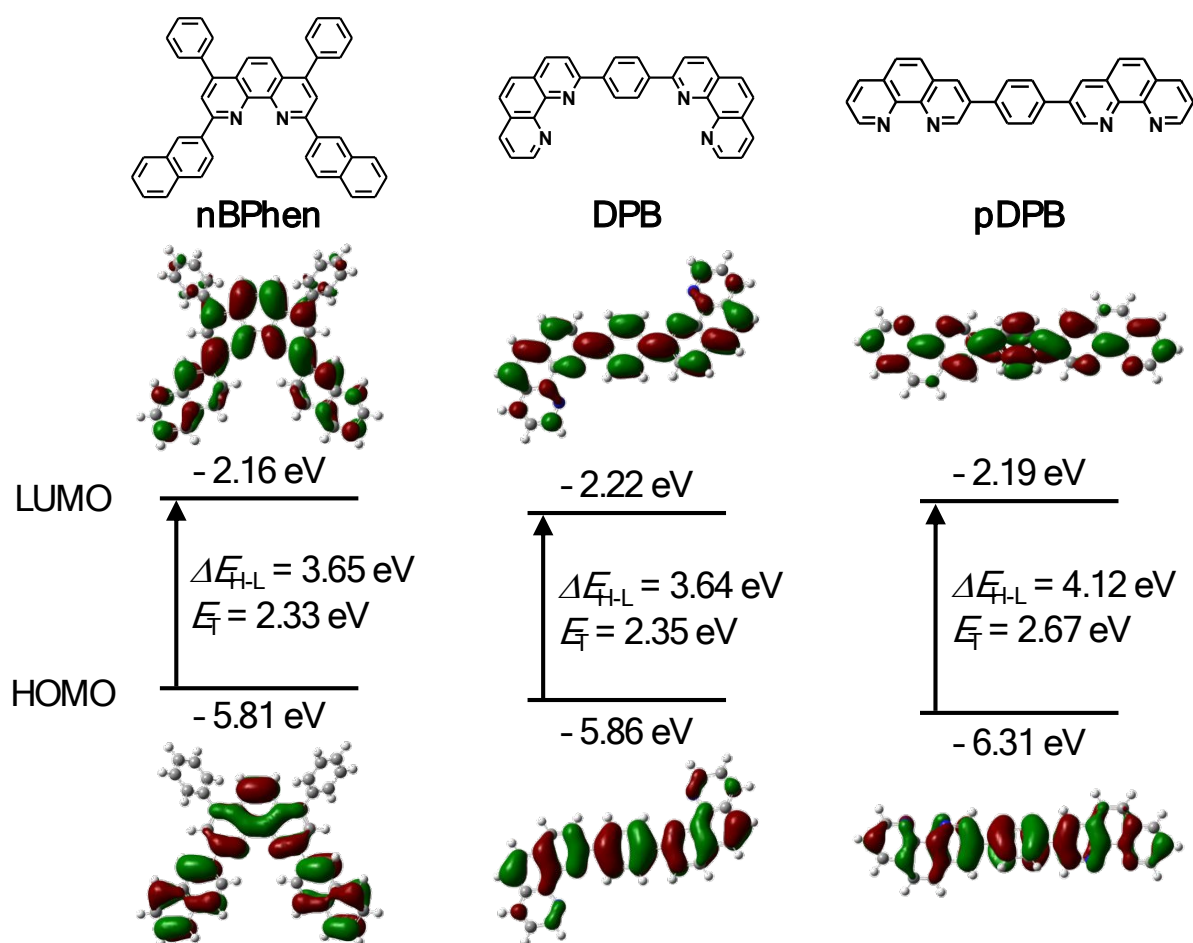
**Figure 1** Chemical structure and the calculated HOMO and LUMO distribution, and T$_1$ levels of **nBPhen**, **DPB**, and **pDPB**.
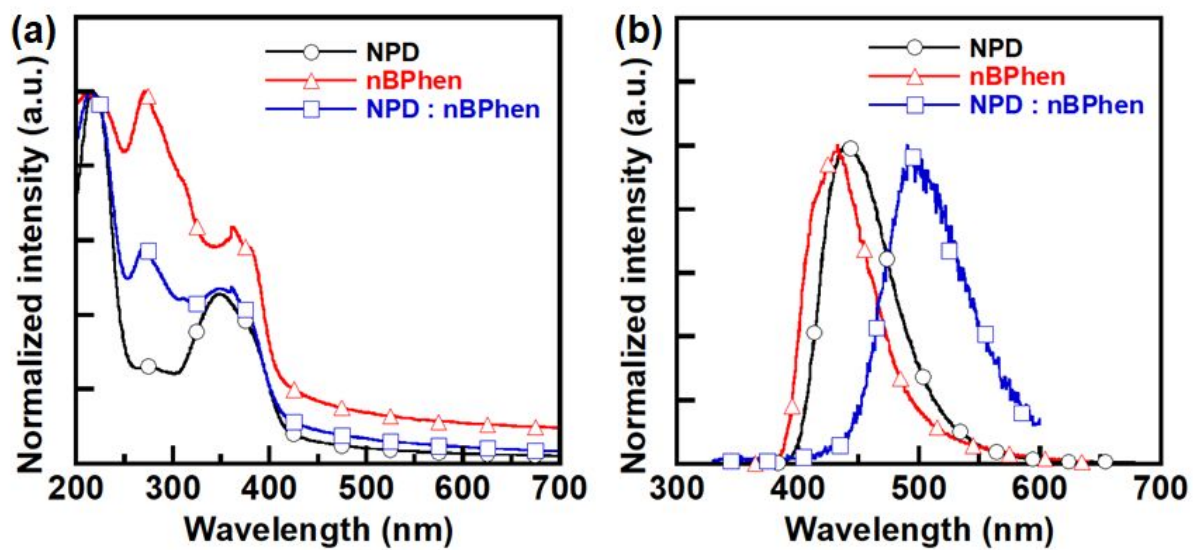
**Figure 2** (a) Normalized UV-Vis absorption and (b) normalized PL spectra of **NPD**, **nBPhen**, and **NPD:nBPhen** (1:1 molar ratio) co-deposited film.

**(a)**



**(b)**



NPD        (DPQ)$_2$Ir(dpm)        Liq
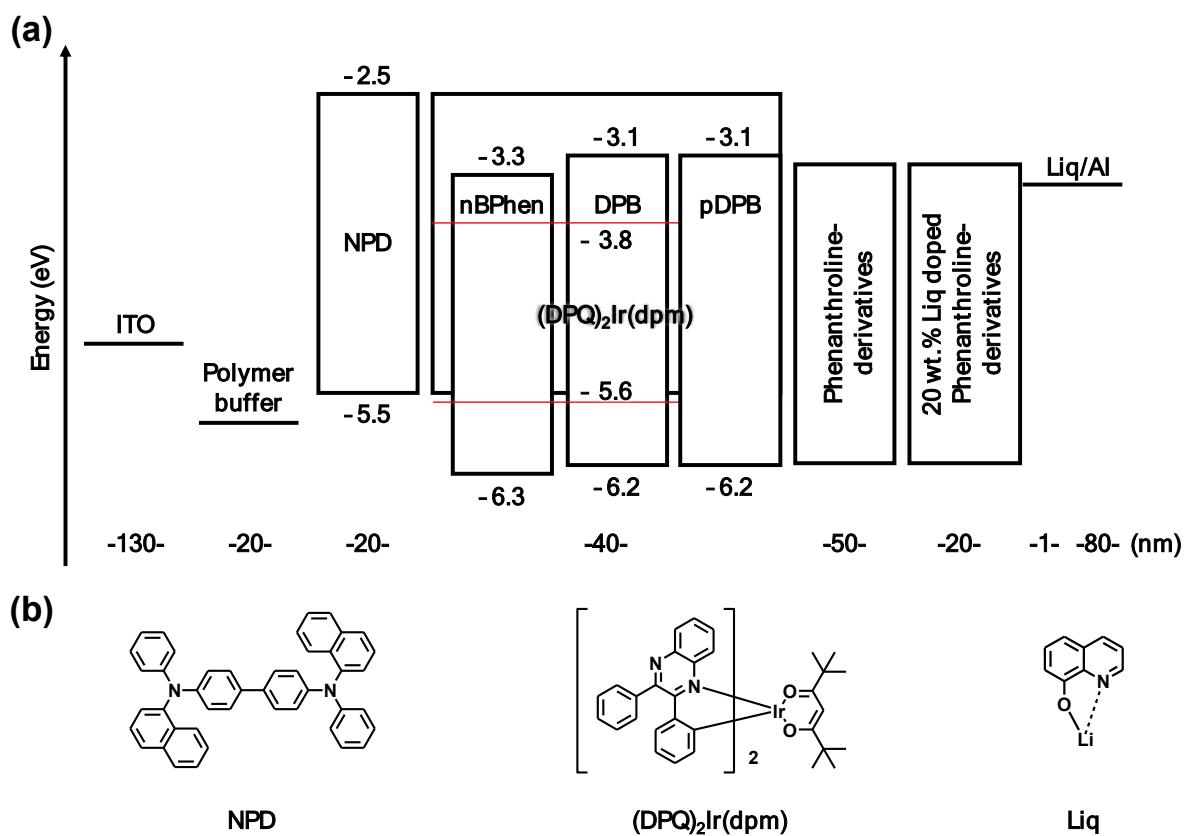
**Figure 3** (a) Energy diagram of the device structure. (b) Chemical structure of used material.
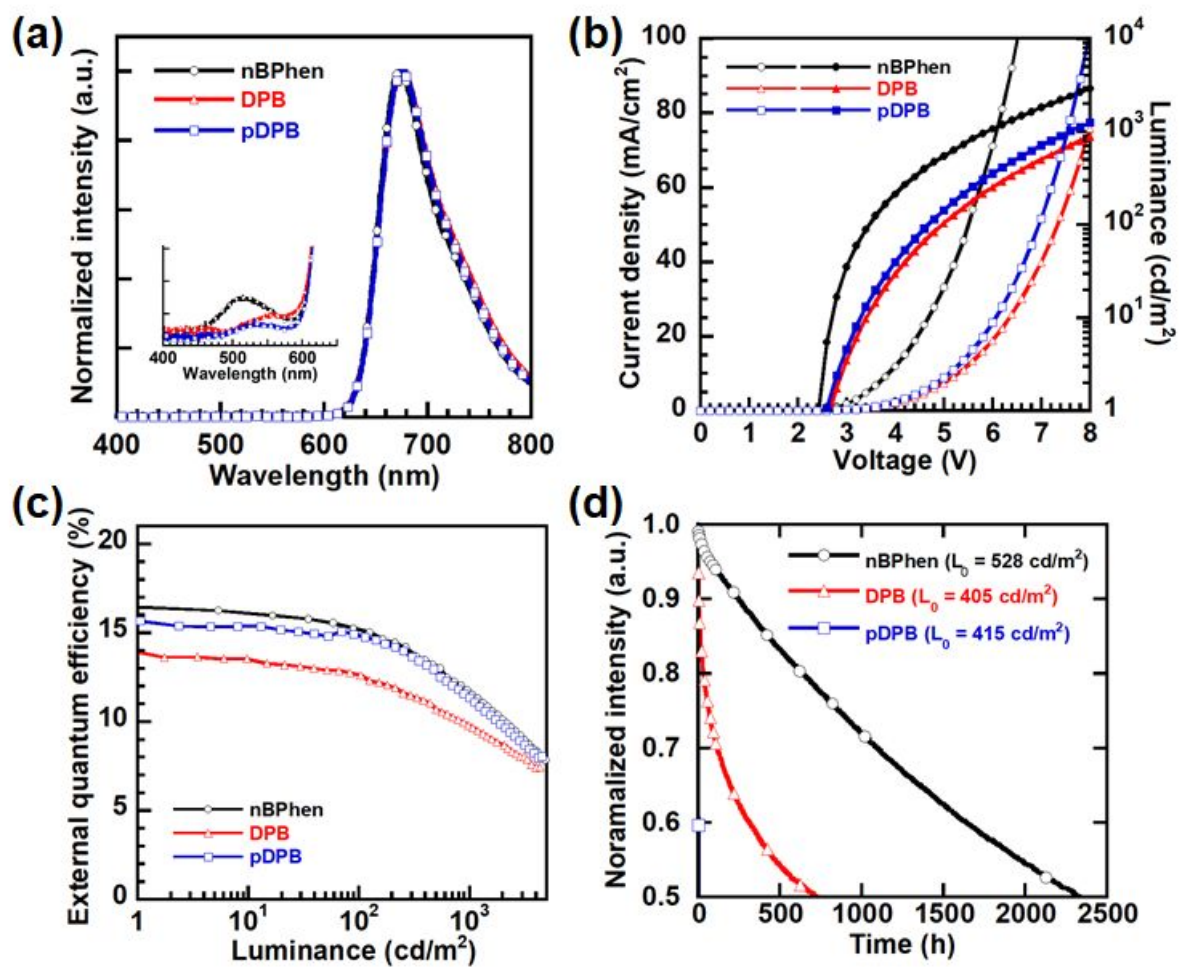
**Figure 4** Device performances: (a) EL spectra at 1 mA (inset: EL spectra of the enlarged short wavelength region), (b) J-V-L characteristics, (c) EQE-L characteristics, and (d) device lifetime under the constant current density of 25 mA cm$^{-2}$.
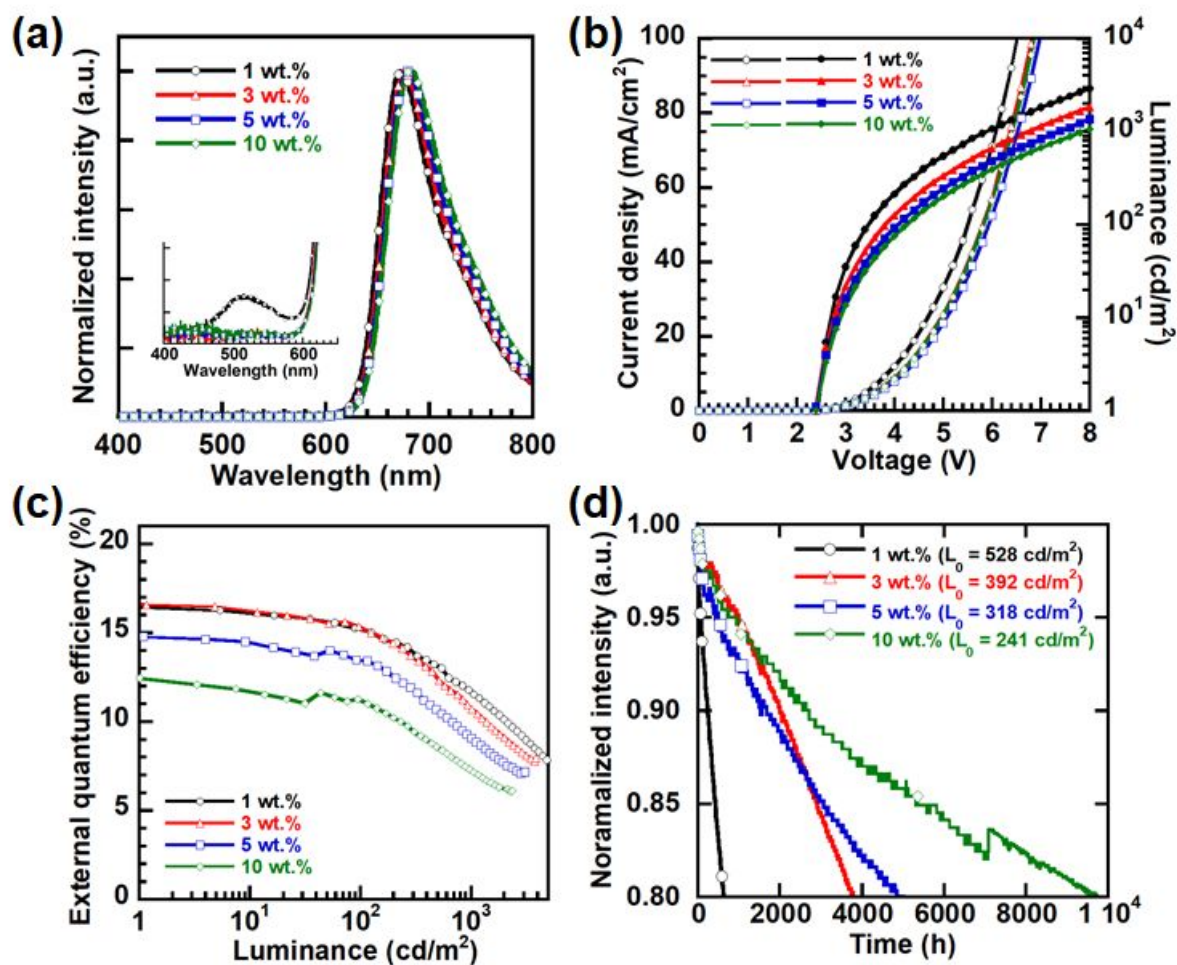
**Figure 5** Device performances: (a) EL spectra at 1 mA (inset: EL spectra of the enlarged short wavelength region), (b) J-V-L characteristics, (c) EQE-L characteristics, and (d) device lifetime under the constant current density of 25 mA cm$^{-2}$.

**Table 1** Physical properties of the phenanthroline derivatives

|  | $T_g$ [a]/$T_m$ [a]/$T_{d5}$ [b] [°C] | HOMO/LUMO/$E_T$ [eV] [c] | $I_p$ [d]/$E_a$ [e]/$E_g$ [f] /$E_T$ [g] [eV] | PLQY [h] [%] |
|---|---|---|---|---|
| nBPhen | 149/349/479 | -5.81/-2.16/2.33 | -6.3/-3.3/3.0/2.37 | 57.4 |
| DPB | n.a./425/480 | -5.86/-2.22/2.35 | -6.2/-3.1/3.1/2.47 | 45.4 |
| pDPB | n.a./366/488 | -6.31/-2.19/2.67 | -6.2/-3.1/3.1/2.92 | 44.7 |

[a] Determined by DSC measurement, [b] obtained from TGA, [c] calculated at the B3LYP/6-311G + (d,p)//B3LYP/6-31G level, [d] obtained from PYS, [e] calculated using $I_p$ and $E_g$, [f] taken as the point of intersection of the normalized absorption spectra, [g] estimated from the onset of phosphorescence spectra, and [h] PLQY values of 1 wt.% $(DPQ)_2Ir(dpm)$-doped NPD:n-type host.

**Table 2** Summary of the OLED performances

|  | $V_{on}$/$PE_{on}$/$CE_{on}$/$EQE_{on}$ [a] [V/lm W$^{-1}$/cd A$^{-1}$/%] | $V_{100}$/$PE_{100}$/$CE_{100}$/$EQE_{100}$ [b] [V/lm W$^{-1}$/cd A$^{-1}$/%] | $V_{1000}$/$PE_{1000}$/$CE_{1000}$/$EQE_{1000}$ [c] [V/lm W$^{-1}$/cd A$^{-1}$/%] | CIE @ 25 mA cm$^{-2}$ | LT$_{80}$ [d] [hs] |
|---|---|---|---|---|---|
| nBPhen | 2.41/2.64/2.02/16.5 | 3.46/1.71/1.88/15.2 | 5.88/0.81/1.52/11.7 | (0.68, 0.29) | 640 |
| DPB | 2.65/1.86/1.56/14.0 | 4.96/0.89/1.41/12.6 | 8.24/0.44/1.14/9.78 | (0.71, 0.29) | 34.3 |
| pDPB | 2.58/2.19/1.80/15.7 | 4.68/1.11/1.65/14.9 | 7.59/0.53/1.29/11.3 | (0.71, 0.29) | 0.303 |

[a] Voltage ($V$), power efficiency (PE), current efficiency (CE), and external quantum efficiency (EQE) at 1 cd m$^{-2}$; [b] V, PE, CE, and EQE at 100 cd m$^{-2}$; [c] V, PE, CE, and EQE at 1000 cd m$^{-2}$; [d] Operational lifetime: 20% decay of initial luminance at current density of 25 mA cm$^{-2}$.

**Table 3** Summary of the OLED performances

|  | $V_{on}$/$PE_{on}$/$CE_{on}$/$EQE_{on}$ [a] [V/lm W$^{-1}$/cd A$^{-1}$/%] | $V_{100}$/$PE_{100}$/$CE_{100}$/$EQE_{100}$ [b] [V/lm W$^{-1}$/cd A$^{-1}$/%] | $V_{1000}$/$PE_{1000}$/$CE_{1000}$/$EQE_{1000}$ [c] [V/lm W$^{-1}$/cd A$^{-1}$/%] | CIE @ 25 mA cm$^{-2}$ | LT$_{80}$ [d] [hs] |
|---|---|---|---|---|---|
| 1 wt.% | 2.41/2.64/2.02/16.5 | 3.46/1.71/1.88/15.2 | 5.88/0.81/1.52/11.7 | (0.68, 0.29) | 640 |
| 3 wt.% | 2.37/2.16/1.63/16.7 | 3.82/1.20/1.46/15.3 | 6.73/0.49/1.06/10.8 | (0.72, 0.28) | 3800 |
| 5 wt.% | 2.38/1.75/1.32/14.8 | 4.07/0.88/1.14/13.4 | 7.38/0.33/0.79/9.09 | (0.72, 0.28) | 5100 |
| 10 wt.% | 2.40/1.38/1.05/12.5 | 4.24/0.63/0.85/11.2 | 7.86/0.22/0.56/7.25 | (0.72, 0.28) | 9840 |

[a] Voltage ($V$), power efficiency (PE), current efficiency (CE), and external quantum efficiency (EQE) at 1 cd m$^{-2}$; [b] V, PE, CE, and EQE at 100 cd m$^{-2}$; [c] V, PE, CE, and EQE at 1000 cd m$^{-2}$; [d] operational lifetime: 20% decay of initial luminance at current density of 25 mA cm$^{-2}$.